Kidney-resident macrophages limit toxin-induced inflammation through their hallmark functions

Minki Hong[1,5], Donghwan Yun[1,2,5], Juhyeon Hwang[1], Chaelin Kang[1], Haein Yoon[1], Suk-Kyung Shin[1], Boyoun Jang[1], Jeongmin Oh[1], Peong Gang Park[3], Hyun Mu Shin[1], Kyung Chul Moon[4], Dong Ki Kim[2], Kook-Hwan Oh[2], Kwon Wook Joo[2], Dong-Sup Lee[1], Yon Su Kim[1,2] and Seung Seok Han[2]

[1]Department of Biomedical Sciences, Seoul National University College of Medicine, Seoul, Korea; [2]Department of Internal Medicine, Seoul National University College of Medicine, Seoul, Korea; [3]Department of Translational Medicine, Seoul National University College of Medicine, Seoul, Korea; and [4]Department of Pathology, Seoul National University College of Medicine, Seoul, Korea

Abstract

Introduction: The inflammatory phenotype of acute kidney injury (AKI), characterized by interstitial infiltration of immune cells, arises due to nephrotoxic agents. However, it does not pose the same risk of occurrence and progression for everyone, suggesting that the amplification or attenuation of disease depends on the unique immunological status of each kidney. Here, our study investigated the regulatory role of kidney-resident macrophages (KRMs) in the induction and progression of toxin-induced AKI.

Methods: To explore this, mice were administered standard pellet chow supplemented, or not, with 0.2% adenine. We injected antibodies against the colony-stimulating factor 1 receptor to selectively depleted KRMs while preserving other kidney-infiltrating macrophages (KiMs) over an extended period owing to different kinetics of KRMs and KiMs.

Results: During the KRM-free period, apoptotic cells accumulated in the interstitium, largely due to the lack of AXL receptor tyrosine kinase, crucial for the efferocytotic function of KRMs. This KRM-free kidney with apoptotic debris induced stress on surrounding tubules, thereby increasing p53 expressing and damage marker (KIM-1)-positive cells. Additionally, KRM-free kidneys presented increased production of chemokine CCL5 from effector $CD8^+$ T cells and increased recruitment of $CCR5^+$ natural killer cells. This occurred because the remaining KiMs, which expressed lower levels of the immune regulatory protein VISTA than did the KRMs, stimulated the effector $CD8^+$ T cells to produce CCL5. The overall alterations in the kidney due to the absence of KRMs ultimately rendered the kidney susceptible to toxin-induced AKI occurrence and progression. Changes in AKI outcomes related to AXL and VISTA expression in kidney mononuclear phagocytes were also observed in human kidney tissues.

Conclusions: Collectively, our findings underscore the hallmark role of KRMs in modulating kidney conditions and mitigating the risk of toxin-induced AKI.

Kidney International (2025) ■, ■–■; https://doi.org/10.1016/j.kint.2025.07.022

KEYWORDS: acute kidney injury; efferocytosis; kidney-resident macrophage; tubulointerstitial nephritis

Translational Statement

Kidney-resident macrophages (KRMs) exhibit unique cellular dynamics, kidney distribution, and differentiation machinery distinct from other macrophages. A hallmark function of KRMs is efferocytotic surveillance, which involves clearing apoptotic debris via AXL and suppressing surrounding T-cell activity through V-domain immunoglobulin suppressor of T-cell activation. These features contribute to tubulointerstitial homeostasis and influence the individual risk of developing and progressing toxin-induced acute kidney injury. KRMs may serve as both predictive and therapeutic targets for toxin-induced acute kidney injury.

The inflammatory phenotype of acute kidney injury (AKI) manifests as tubulointerstitial nephritis (TIN), characterized by immune cell infiltration and tubulitis, while the glomeruli and vessels are relatively spared.[1] The histologic presence of interstitial immune cell infiltration clearly indicates that inflammatory AKI is a representative immune-mediated disease often triggered by toxins, drugs, and other factors.[2,3] Recently, inflammatory AKI has garnered attention because of its association with novel therapeutic agents, such as immune checkpoint inhibitors, as a renal adverse event that necessitates treatment interruption until recovery.[4] The risk of AKI occurrence and progression following specific insults varies among individuals,

Correspondence: *Seung Seok Han, Department of Internal Medicine, Seoul National University College of Medicine, 103 Daehak-ro, Jongno-gu, Seoul, 03080, Korea. E-mail: hansway7@snu.ac.kr*

[5]MH and DY are cofirst authors.

Received 25 November 2024; revised 11 June 2025; accepted 14 July 2025

suggesting that unique immunologic status of each kidney plays a crucial role.[5,6] Individual components of the kidney may independently contribute to the development and progression of toxin-induced AKI. If this issue is not addressed, it will be challenging to establish treatments tailored to the underlying immunologic status, and the responsiveness to corticosteroids or other immunoregulative therapies may also vary.[7,8]

Tissue-resident immune cells play a tissue-specific role in maintaining immunologic homeostasis during their residency.[9,10] Specifically, tissue-resident macrophages and memory T cells are recognized as the first layer of protection against harmful microorganisms, with greater emphasis placed on their role in infection rather than their noninfectious roles.[11] In mouse kidneys, most resident immune cells are kidney-resident macrophages (KRMs),[6,12] and they consistently reside in the tubulointerstitial area even during inflammation.[13,14] These cells regulate the extent of injury in addition to initiating inflammation, as evidenced by their dual proinflammatory and anti-inflammatory signatures at baseline.[15,16] This tuning function has been particularly demonstrated in noninfectious injury models,[13,15] although the underlying mechanisms remain largely unexplored, in addition to specific molecule-dependent processes.[17] Further research on aspects of KRMs other than their residency is warranted because their recovery process is likely to involve characteristics distinct from those of other heterogeneous kidney-infiltrating macrophages (KiMs). A prime example is the phagocytic function of KRMs, which differs from that of other KiMs, and this difference influences the overall course of the inflammatory process or the spontaneous occurrence of kidney-specific disorders.[18,19] These findings suggest a homeostatic function for KRMs and anticipate their potential impact, particularly on the individualized occurrence of kidney-specific inflammatory conditions. Therefore, efforts to identify the hallmark functions of KRMs, rather than merely focusing on their proinflammatory or anti-inflammatory phenotypes, could broaden our insights into kidney health and disease.

Current knowledge on the homeostatic role of tissue-resident macrophages suggests that the presence of KRMs and their surveillance within the kidney may contribute to resistance to occurrence and progression of toxin-induced AKI. To explore this hypothesis, an approach involving the long-term and selective depletion of KRMs while preserving other KiMs is essential. However, genetic targeting methods using transgenic mice face challenges because of the presence of shared genes, such as *LyzM*, *Itgax*, *Ccr2*, *Cx3cr1*, and *Ms4a3*, with KiMs and other myeloid cells.[13,20] One effective strategy for exclusively depleting KRMs is to exploit differences in the cellular dynamics between KRMs and KiMs; notably, KRMs have a longer residency period through self-renewal than KiMs do.[21] The repletion dynamics of KRMs after depletion differ from those of other tissue-resident macrophages.[22] The residency period varies between tissues and is influenced by niche conditions, with kidneys having an intermediate residency period compared with the brain and liver, which have long and short periods, respectively.[22,23] Leveraging such cellular dynamics would ultimately deplete KRMs for the desired duration while allowing ready replenishment of KiMs to remain present in the interstitial niche.

Unlike previous studies that depleted KRMs for short durations, ranging from a few days to 1 or 2 weeks,[13,24,25] the present study devised a method to deplete KRMs over a long-term period exceeding 6 weeks using an anti–colony-stimulating factor 1 receptor antibody (αCSF1R Ab) while preserving KiMs.[26] When KRMs were absent for an extended period, the KiMs that filled the niche were not able to fully compensate for the functions of the KRMs. A notable consequence of this was the accumulation of apoptotic debris due to inadequate efferocytosis by KiMs, which express low levels of AXL, a characteristic feature of KRMs. This deficiency led to increased p53 expression and the presence of damage markers in the surrounding tubular cells. Other immunologic changes included increased levels of C-C motif chemokine ligand (CCL) 5 produced by effector $CD8^+$ T cells, resulting in the infiltration of C-C chemokine receptor (CCR) type 5–positive natural killer (NK) cells into the kidney. This process was facilitated through altered interactions between KRMs or KiMs and effector $CD8^+$ T cells, where V-domain immunoglobulin suppressor of T-cell activation (VISTA) might play a role. All of these changes resulting from the prolonged absence of KRMs contributed to an exaggerated progression of AKI induced by foreign toxins. Collectively, KRMs, unlike KiMs, may serve a homeostatic function by regulating excessive inflammation through specialized efferocytosis and by imparting inhibitory signals to neighboring T cells, which are mediated by AXL and VISTA molecules, respectively.

METHODS

Mice

C57BL/6 and *Rag1*$^{-/-}$ mice were purchased from the Jackson Laboratory. C57BL/6 *Axl*$^{-/-}$ mice were provided by Professor Q6 Jongsun Park (College of Medicine, Chungnam National University). C57BL/6 *Vsir*$^{-/-}$ mice were established and bred with a cryopreserved sperm (KOMP Repository, University of California, Davis). All of the mice used in the experiments were 8 weeks of age and male. The animals were housed under specific pathogen-free conditions at the facility of Seoul National University College of Medicine. All animal experiments were approved by the Seoul National University Institutional Animal Care and Use Committee (21-0244-S1A1). The study was conducted in accordance with national guidelines on animal experimentation.

To construct a toxin-induced AKI model, the mice were administered standard pellet chow supplemented with 0.2% adenine (Sigma-Aldrich) beginning on day 0. Kidneys were harvested at the indicated time points (e.g., 0, 7, 14, 21, and 28 days) after perfusion with saline. The control mice were provided a diet without adenine. For another toxin-induced

AKI model, the mice were administered 250 mg/kg of folic acid once via i.p. injection.

Human kidney samples

Normal human kidney tissues were obtained from patients who underwent radical nephrectomy because of urogenital tumors but did not have hydronephrosis or infectious diseases (n = 7). Biopsied kidney tissues were collected from patients with toxin-induced AKI, who showed TIN findings on histologic examination without evidence of other disease entities (n = 27). Immunohistochemistry and immunofluorescence were used to assess the areas of $CD68^+$, AXL^+, and $VISTA^+$ expression in the cortex. The fluorescence intensity of AXL or VISTA in each $CD68^+$ cell was quantified using Imaris software (version 10.2; Bitplane), with a minimum of 50 $CD68^+$ cells analyzed per section. Samples were stratified into KRM^{high} and KRM^{low} groups based on the median value of the KRM fraction among $CD68^+$ cells. Composite renal risk (e.g., doubling of serum creatinine, 50% decrease in estimated glomerular filtration rate, or progression to end-stage kidney disease) was compared between the KRM^{high} and KRM^{low} groups. The study design for human samples was approved by the institutional review board of Seoul National University Hospital (H-2001-084-1095) and complied with the Declaration of Helsinki. All patients provided written informed consent for the donation and use of their samples.

Statistical analysis

All analyses and calculations were performed using GraphPad Prism software (version 8.0; GraphPad Software, Inc.). The data are presented as the mean ± SEM or proportion. Differences between groups were evaluated using Student *t* test for comparisons between 2 groups and analysis of variance (1 or 2 way) with Tukey test for comparisons among multiple groups. Correlation coefficients were measured using Pearson correlation test. Survival curves were drawn using the Kaplan-Meier method. To compare survival curves between groups, a log-rank test was applied. $P < 0.05$ was considered statistically significant. For single-cell RNA (scRNA) sequencing, Bonferroni correction was applied to account for multiple testing, yielding adjusted *P* values.

The antibodies and primers are listed in Supplementary Tables S1 and S2, respectively. Additional methods can be found in Supplementary Methods.

RESULTS

Depletion and repletion of KRMs

Noninjured kidneys harbor 2 subsets of kidney macrophages, namely KRM and KiM, distinguished by their expression patterns of F4/80 and CD11b: KRM, $CD45^+$ $Ly6G^-$ $CD11b^{int}$ $F4/80^{high}$; and KiM, $CD45^+$ $Ly6G^-$ $CD11b^{high}$ $F4/80^{int}$[13,15,18] (Figure 1a). The KiM subset exhibited heterogeneity based on the expression of Ly6C and major histocompatibility complex class II, whereas the KRM subset was homogeneous, expressing $Ly6C^-$ major histocompatibility complex class II^{high}. Following depletion of macrophages via αCSF1R Ab injection, both $F4/80^+$ KRMs and KiMs were almost absent within the third day, whereas the long-term of KRMs and KiMs varied (Figure 1b and c and Supplementary Figure S1). Specifically, KRMs were nearly absent within the kidney starting from the seventh day and began to reappear after 6 weeks. Although KiMs were initially depleted by αCSF1R Ab injection, they promptly started to occupy the KRM-absent interstitial niche, becoming the sole macrophage subset in the kidney for up to 6 weeks. Ultimately, at 3 months after αCSF1R Ab injection, the proportion of KRMs within the kidney was restored to a level similar to that of mice treated with control Ab (Figure 1d). This cellular dynamic did not affect the proliferation potential of the KRMs or KiMs, which exhibited low (i.e., <5%) and high rates, respectively (Figure 1e and f). The morphology and size of the original and repleted KRMs remained similar (Figure 1g). We then exploited this KRM-free condition to evaluate the homeostatic role of KRMs, particularly in normal kidneys, before toxin-induced AKI induction.

Distinct distribution of kidney macrophages during repletion

The kidney is structurally divided into the cortex and medulla, both of which contain interstitial areas that serve as niches for macrophages.[27] However, the volumes of the interstitial area and their interactions with the parenchyma differ between these 2 regions, leading to structurally distinct immunologic homeostasis.[12,18,28] Before depleting the KRMs (i.e., day 0), these macrophages were more distributed in the medulla than in the cortex (Figure 2a and b). During the repletion period, KiMs primarily occupied the interstitial areas of the cortex rather than the medulla, resulting in a reversal of the cellular distribution ratio after depletion. Over time, this ratio gradually normalized, with an increasing presence of macrophages in the medulla (Figure 2c). This characteristic distribution may partly result from alterations in the chemokine ligands released from the macrophage-depleted kidneys.[29] To explore this further, we examined the expression of representative chemokine receptors for KRMs and KiMs, specifically CCR2 and C-X3-C motif chemokine receptor 1 (CX3CR1).[30] Most KRMs and 80% of KiMs expressed CX3CR1, with similar expression patterns observed in the control Ab-treated and αCSF1R Ab–treated groups (Figure 2d). With respect to CCR2 expression, the CCR2-positive subset increased in the KRMs during the repletion phase, whereas the KiMs showed no difference in CCR2 expression before and after depletion. These results suggest that over time, there is a transition from a CCR2-negative KRM subset, originating from the yolk sac and fetal liver, to a CCR2-positive subset derived from the bone marrow.[30–32]

We subsequently compared the gene expression levels of chemokine ligands targeting CCR2, CX3CR1, and C-X-C chemokine receptor type 4 on day 7 after Ab injection because KiMs are known to express these receptors (Figure 2e).[21,33] Ligands targeting CCR5 were also evaluated

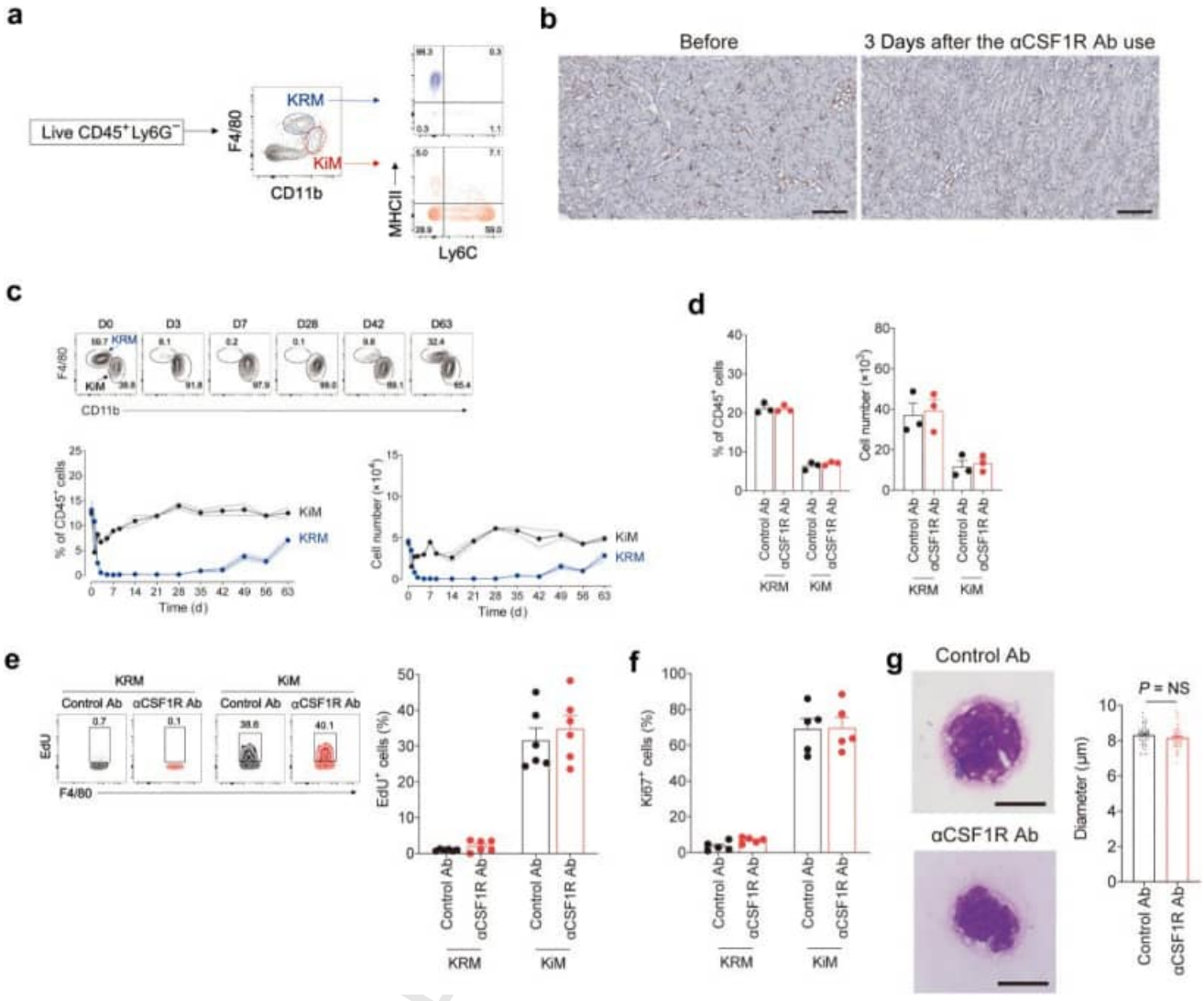

Figure 1 | Cellular dynamics after macrophage depletion with anti–colony-stimulating factor 1 receptor antibody (αCSF1R Ab). (**a**) Representative flow cytometry plot of kidney-resident macrophages (KRMs) and kidney-infiltrating macrophages (KiMs). (**b**) Representative images stained for F4/80 before and 3 days (D) after αCSF1R Ab treatment. Bars = 100 μm. (**c**) Representative flow cytometry plot of KRMs and KiMs before and after αCSF1R Ab use, and their proportions among kidney immune cells and cell numbers per kidney (n = 5∼6 per time point). (**d**) Proportions and cell numbers of KRMs and KiMs 3 months after αCSF1R Ab use (n = 3 per group). (**e**) Representative flow cytometry plot of EdU$^+$ cells per KRM or KiM after αCSF1R Ab or control Ab treatment, and comparison of EdU$^+$ cells between KRMs and KiMs (n = 6 per group). (**f**) Comparison of Ki67$^+$ cells between KRMs and KiMs. (**g**) Giemsa staining of KRMs 42 days after αCSF1R Ab or control Ab use, and comparison of their size between the αCSF1R Ab and control Ab groups. The cell size was calculated from 50 cells sorted from the kidneys of 3 mice. Bars = 5 μm. NS, not significant. To optimize viewing of this image, please see the online version of this article at www.kidney-international.org.

for reference because this receptor is expressed primarily in kidney-infiltrating lymphocytes.[34] The gene expression of *Ccl2* and *Ccl7*, which target CCR2, and *Cx3cl1*, which targets CX3CR1, appeared to increase in the αCSF1R Ab–treated kidneys, with the most significant change observed in the *Ccl2* gene. The expression of *Ccl12*, which targets CCR2, and *Ccl3*, *Ccl4*, and *Ccl5*, which target CCR5, decreased. These trends were observed in both the cortex and medulla substructures. The protein expression of CCL2 was greater in the αCSF1R Ab–treated kidneys than in the control Ab-treated kidneys, particularly in the cortex rather than in the medulla (Figure 2f and g). The gene expression of growth factors targeting CSF1R, such as CSF1 and interleukin 34, did not change after αCSF1R Ab injection (Figure 2h). After blocking the CCL2-CCR2 axis with αCCL2 Ab, reductions in KRMs during the repopulation period, as well as in overall macrophage infiltration during the early phase, were observed (Figure 2i and j). Collectively, consistent with previous reports,[18,30] the CCL2-CCR2 axis is involved not only in macrophage infiltration into the interstitial niche but also in the repopulation of KRMs.

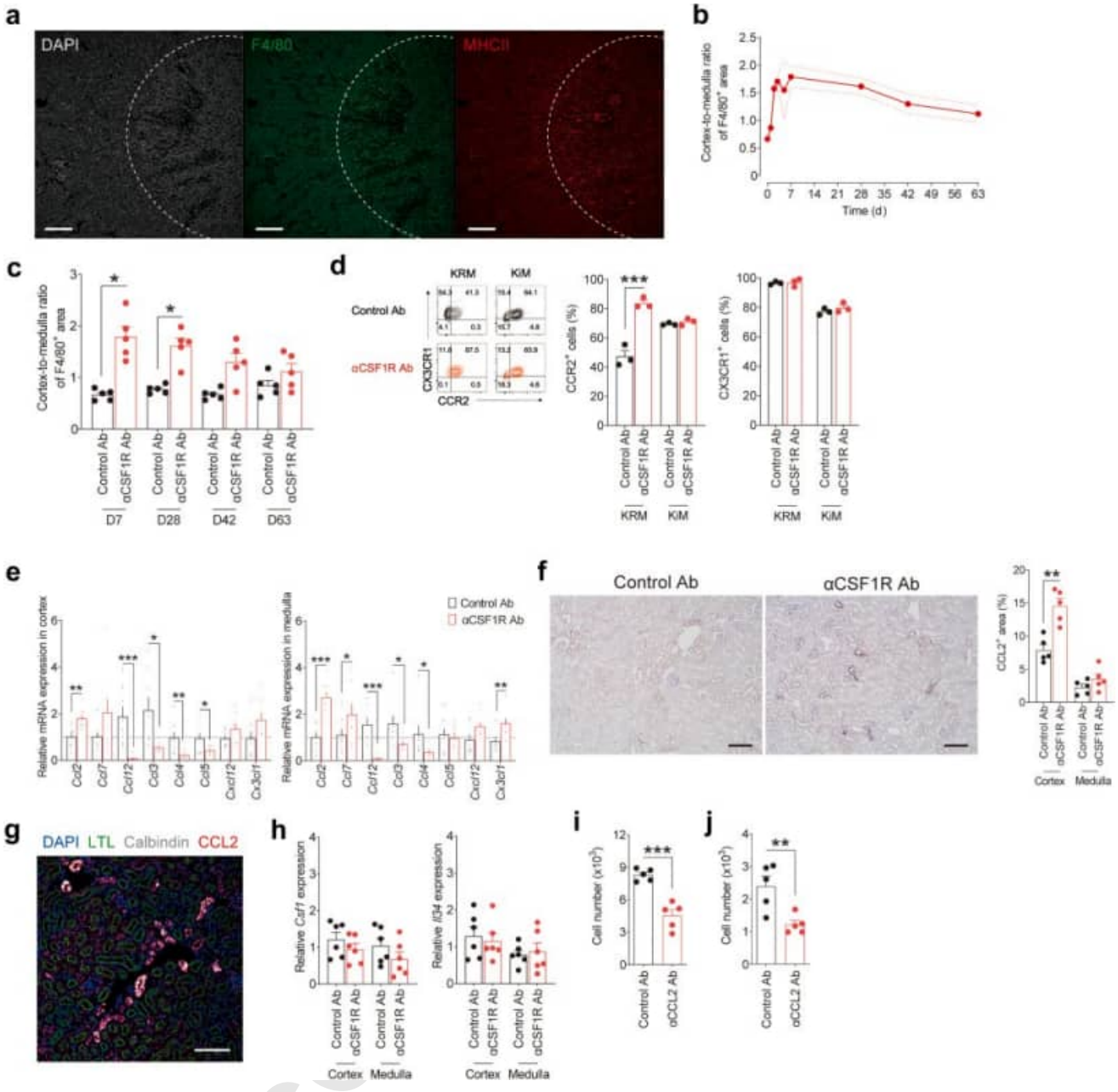

Figure 2 | Distribution of kidney macrophages during repletion. (**a**) Representative images stained for 4′,6-diamidino-2-phenylindole (DAPI), F4/80, and major histocompatibility complex class II (MHCII) to visualize the distribution of kidney-resident macrophages (KRMs) in baseline kidneys. Dashed lines indicate the boundary between the cortex (left) and medulla (right). Bars = 200 μm. (**b**) Ratio of the F4/80$^+$ area between the cortex and medulla. (**c**) Cortex-to-medulla ratio of the F4/80$^+$ area at different time points (n = 5 per time point). (**d**) Representative flow cytometry plot of C-C chemokine receptor 2 (CCR2) and C-X3-C motif chemokine receptor 1 (CX3CR1) positivity in kidney macrophage subsets after treatment with anti–colony-stimulating factor 1 receptor antibody (αCSF1R Ab) or control Ab, and comparison of CCR2 and CX3CR1 positivity between the αCSF1R Ab and control Ab treatments (n = 3 per group). (**e**) Gene expression of chemokine ligands targeting CCR2, CCR5, CX3CR1, and C-X-C chemokine receptor type 4 on day (D) 7 after Ab injection in the kidney parenchyma. (**f**) Representative images of kidney sections immunostained for C-C motif chemokine ligand 2 (CCL2) on day 7 after Ab injection, and comparison of the CCL2$^+$ area between the αCSF1R Ab– and control Ab-treated groups (n = 5 per group). Bars = 100 μm. (**g**) Representative image of kidney sections immunostained for DAPI, lotus tetragonolobus lectin (LTL), calbindin D28k, and CCL2. Bar = 100 μm. (**h**) Gene expression of chemokine ligands targeting CSF1R on day 7 after Ab injection in the kidney parenchyma (n = 5 per group). (**i**) Kidney-infiltrating macrophage (KiM) cell numbers following treatment with αCCL2 Ab, compared with control Ab treatment, on day 14 after αCSF1R Ab administration (n = 5 per group). The Ab was administered i.p. at a dose of 200 μg/kg 4 times after αCSF1R Ab treatment, and cell numbers were evaluated on day 14. (**j**) Comparison of repopulated KRM numbers between αCCL2 Ab and control Ab treatments (n = 5 per group). The Ab was administered i.p. at a dose of 200 μg/kg twice per week, starting on day 42 after αCSF1R Ab treatment, and cell numbers were evaluated on day 63. *$P < 0.05$, **$P < 0.01$, ***$P < 0.001$. To optimize viewing of this image, please see the online version of this article at www.kidney-international.org.

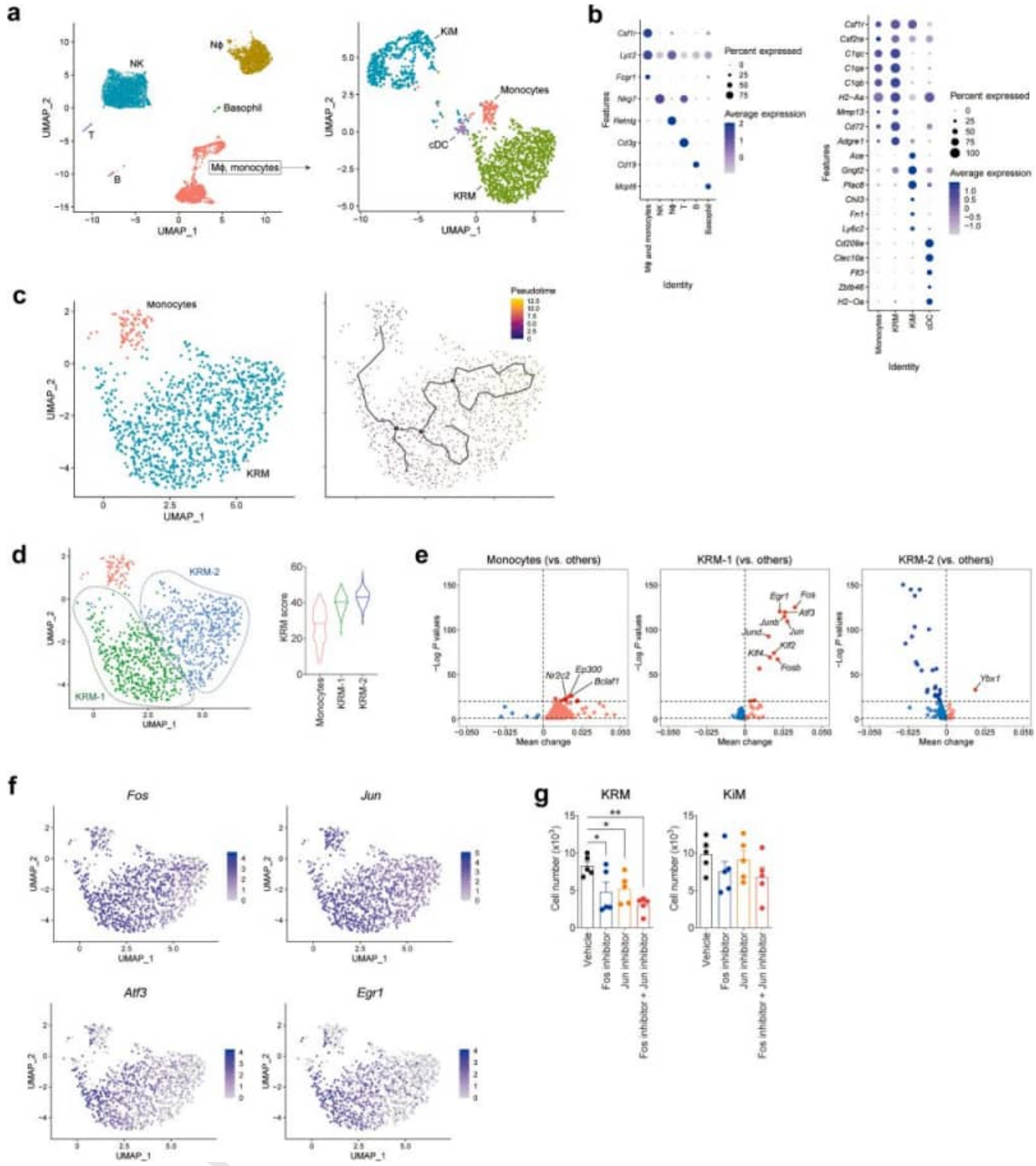

Figure 3 | Differentiation of kidney-resident macrophages (KRMs) from monocytes during repletion. (**a**) Uniform Manifold Approximation and Projection (UMAP) plots of 7596 CD11b-positive immune cells on day 42 after αCSF1R Ab injection. (**b**) Dot plots to identify clusters of immune cells. (**c**) UMAP plots after subclustering monocytes and KRMs (left) and pseudotime trajectories of cells (right). The black line represents the trajectory graph when the starting point is set in the monocyte cluster, and the roots are marked as circles. (**d**) UMAP plot of the 2 groups of KRMs (left) and a violin plot illustrating changes in the KRM signature score among the monocyte and KRM groups. (**e**) SCENIC analysis results identifying transcription factors related to the genetic profile of each cluster. (**f**) UMAP plots with expression patterns of transcription factor genes primarily expressed in the KRM-1 cluster. (**g**) Cell number of kidney macrophage subsets per kidney during repletion after the use of inhibitors against Fos and Jun transcription factors. *$P < 0.05$, **$P < 0.01$. cDC, classic dendritic cell; KiM, kidney-infiltrating macrophage; Mϕ, macrophage; NK, natural killer; Nϕ, neutrophil.

FLA 5.7.0 DTD ■ KINT4344_proof ■ 4 September 2025 ■ ce

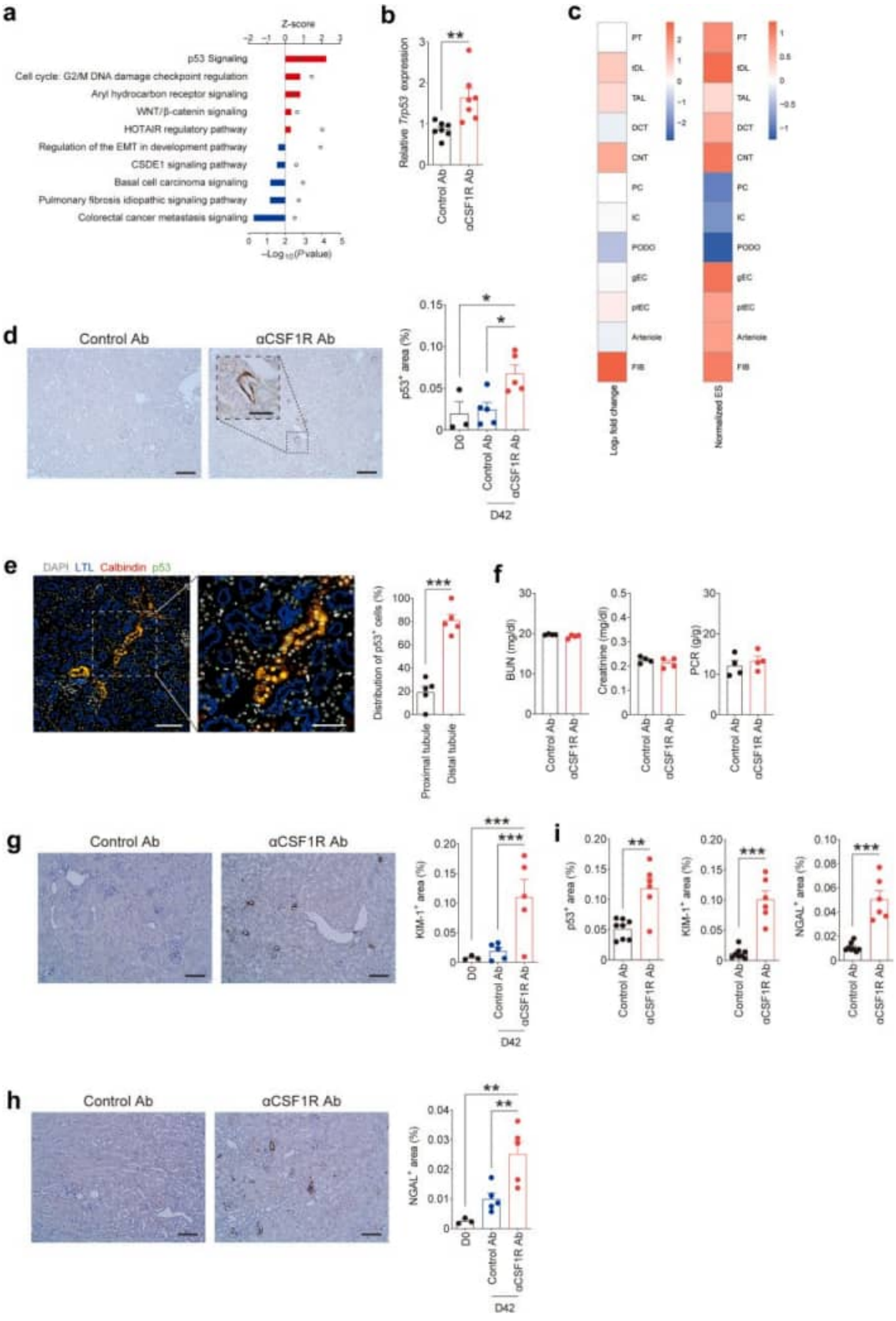

Figure 4 | Changes in parenchymal tissue during the kidney-resident macrophage–absent period. (**a**) Ingenuity pathway analysis results using kidney parenchyma on day (D) 42 after anti–colony-stimulating factor 1 receptor antibody (αCSF1R Ab) injection compared with control Ab injection (n = 3 per group). Bars and circles represent Z-score and –log10(*P* value), respectively. (**b**) Expression of the *Trp53* gene in the kidney parenchyma in the αCSF1R Ab– and control Ab-treated groups (n = 7 per group). (**c**) Heat map of *Trp53* gene (continued)

Differentiation of KRMs during repletion

Tissue-resident macrophages are influenced by distinct transcription factors for differentiation and maintenance in each organ,[35,36] which may affect their expression patterns and functions to meet the specific needs of each organ.[9,21] Under homeostatic and quiescent conditions, bone marrow–derived KRMs depend on certain transcription factors, such as MYB.[23,37] The transcriptional programming of these macrophages may exhibit high plasticity, particularly in response to changes in the interstitial niche or surrounding tissue.[38–40] To identify transcription factors related to the repletion phase, scRNA sequencing data were obtained when KRMs began to repopulate the interstitial niche (i.e., day 42 after the administration of the αCSF1R Ab) (Figure 3a and b). A trajectory analysis was performed on the data, focusing on 2 clusters: monocytes and KRMs (Figure 3c). For the KRMs, 2 additional clusters emerged, which we labeled KRM-1 and KRM-2 (Figure 3d). When we calculated scores based on KRM signature genes, we observed a sequential increase in scores from the monocyte cluster to the KRM-2 cluster. Notably, a transient increase in a gene set of transcription factors, including *Fos*, *Jun*, *Atf3*, and *Egr1*, was observed in the KRM-1 cluster during differentiation (Figure 3e and f). These transcription factors are known to be involved in the differentiation of monocytes into macrophages, although they may not function alone.[41–43] When inhibitors against Fos or Jun were administered during the repletion phase, KRM differentiation was abrogated (Figure 3g). Taken together, the machinery of transcription factors is crucial for KRM differentiation within a specific niche condition, particularly after long-term depletion of KRMs. Although the current models do not reflect disease conditions, this finding provides a basis for understanding similar conditions in noninjured kidneys and may offer insights into the regulation of KRM differentiation.

Efferocytotic surveillance of KRMs

Analyzing changes in the surrounding parenchymal tissue when the KRM is absent may confirm the homeostatic role of KRMs. To achieve this goal, bulk transcriptomics were initially performed on kidneys on day 42 after the administration of either αCSF1R Ab or control Ab. Pathway analysis revealed that the most significant change in αCSF1R Ab–treated parenchymal tissues was an increase in p53 signaling (Figure 4a). This finding was further validated through quantitative polymerase chain reaction, scRNA sequencing, and immunohistochemistry (Figure 4b–d). p53 Signaling was more dominant in distal tubules than in proximal tubules (Figure 4e). p53 Signaling is a key component of the cellular response to stress, which induces apoptosis and cell cycle arrest in kidney tubules.[44,45] Biomarkers for kidney injury at the macro level, such as blood urea nitrogen, serum creatinine, and proteinuria, remained within normal ranges and did not differ between the αCSF1R Ab–treated and control Ab-treated kidneys (Figure 4f). However, despite the absence of overt kidney dysfunction, the αCSF1R Ab–treated kidneys exhibited increased expression of kidney injury molecule-1 and neutrophil gelatinase-associated lipocalin, indicating the presence of subclinical injury in the absence of KRMs (Figure 4g and h). The expression of injury markers was not confined to p53-positive tubules (Supplementary Figure S2). We established kidney conditions without KRMs for up to 18 weeks by administering αCSF1R Ab 3 times at 6-week intervals (Supplementary Figure S3). Parenchymal changes, including the upregulation of p53 and damage markers, were pronounced in this extended KRM-depleted condition (Figure 4i).

To understand why the absence of KRMs induces p53 signaling in surrounding tissue and leads to subclinical damage, we evaluated the phagocytic capacity, a hallmark function of macrophages, which may differ between KRMs and KiMs. Initially, we assessed the presence of apoptotic debris in the kidneys, which was increased in the αCSF1R Ab–treated kidneys compared with the control Ab-treated kidneys (Figure 5a). This accumulation of apoptotic debris was further pronounced in the KRM-depleted kidneys when the depletion was extended to 18 weeks (Supplementary Figure S4). The overall transcriptomic profile of KRMs was more associated with B-cell–mediated immunity and

Figure 4 | (continued) expression in the αCSF1R Ab–treated kidneys relative to the control Ab-treated group, based on single-cell RNA sequencing data of sorted $CD45^+$ cells. Expression ratios are presented as $\log_2$ fold changes (left) and normalized enrichment scores (ESs) from pathway analysis. (**d**) Representative plots of kidney sections immunostained for p53 on day 42 after Ab injection, and comparison of the $p53^+$ area between the αCSF1R Ab– and control Ab-treated groups (n = 5 per group). Bars = 100 μm. (**e**) Representative image of αCSF1R Ab–treated kidney sections immunostained for 4′,6-diamidino-2-phenylindole (DAPI), lotus tetragonolobus lectin (LTL), calbindin D28k, and p53. Merged cells for calbindin and p53 are shown in orange. Bars = 100 μm (left) and 50 μm (right). The bar graph indicates the proportion of $p53^+$ cells within the tubular subset. (**f**) Biomarkers for kidney injury at the macro level on day 42 after Ab injection. (**g**) Representative plots of kidney sections immunostained for kidney injury molecule-1 (KIM-1) on day 42 after Ab injection, and comparison of tubular $KIM\text{-}1^+$ area between the αCSF1R Ab– and control Ab-treated groups (n = 5 per group). Bars = 100 μm. (**h**) Representative plots of kidney sections immunostained for neutrophil gelatinase–associated lipocalin (NGAL) on day 42 after Ab injection, and comparison of tubular $NGAL^+$ area between the αCSF1R Ab– and control Ab-treated groups (n = 5 per group). Bars = 100 μm. (**i**) Comparison of the $p53^+$, $KIM\text{-}1^+$, and $NGAL^+$ areas between the αCSF1R Ab– and control Ab-treated groups after Ab administration 3 times every 6 weeks (n = 6∼8 per group). $^*P < 0.05$, $^{**}P < 0.01$, $^{***}P < 0.001$. BUN, blood urea nitrogen; CNT, connecting tubule; CSDE, xxx; DCT, distal convoluted tubule; EMT, epithelial-to-mesenchymal transition; FIB, fibroblast; gEC, glomerular endothelial cell; IC, intercalated cell of collecting duct; PC, principal cell of collecting duct; PCR, random urine protein-to-creatinine ratio; PODO, podocyte; PT, proximal tubule; ptEC, peritubular endothelial cell; TAL, thick ascending limb; tDL, thin descending limb. To optimize viewing of this image, please see the online version of this article at www.kidney-international.org.

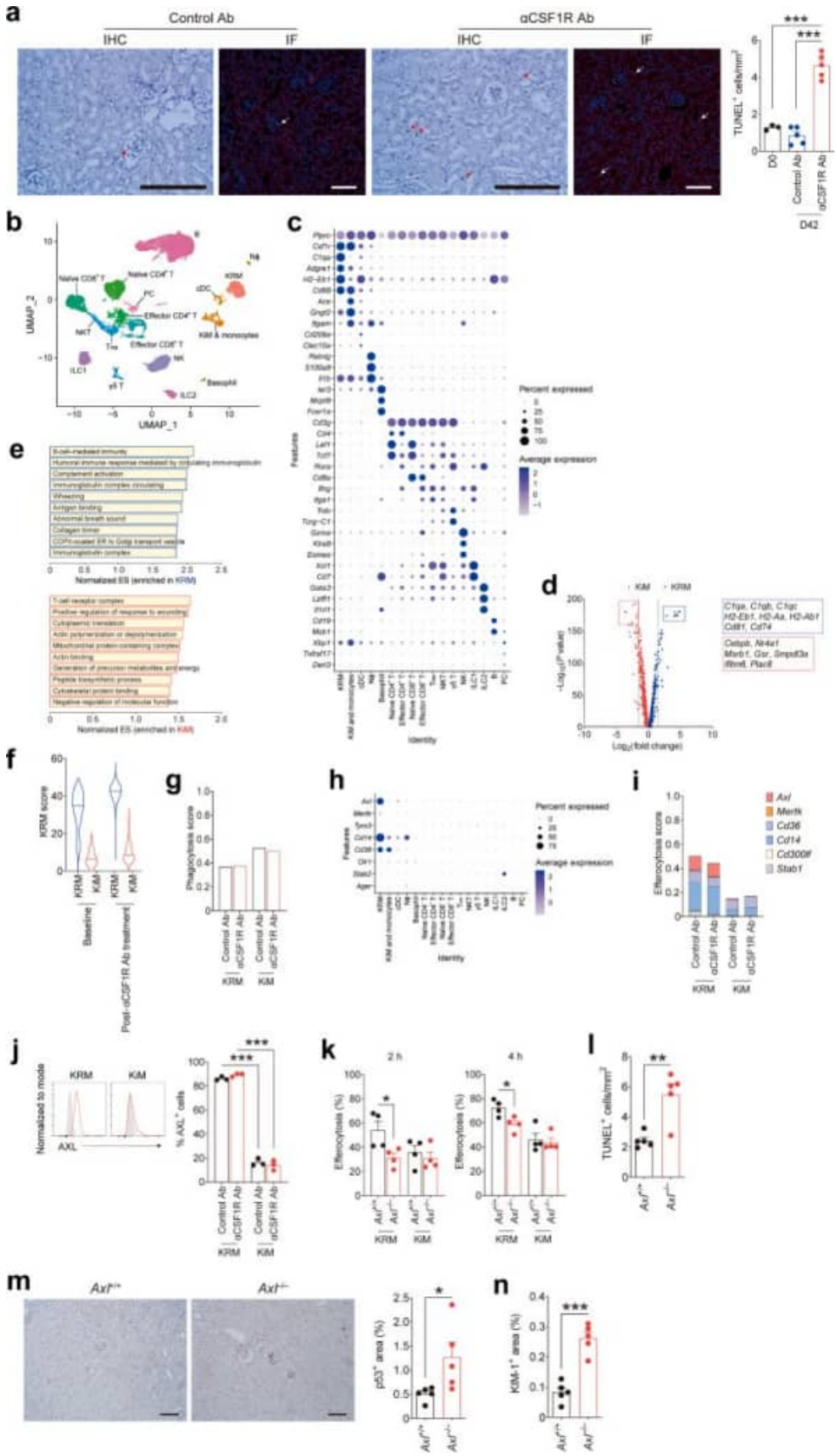

Figure 5 | Efferocytotic signature of kidney-resident macrophages (KRMs). (**a**) Representative terminal deoxynucleotidyl transferase–mediated dUTP nick end-labeling (TUNEL) images of kidneys on day (D) 42 after antibody (Ab) injection via immunohistochemistry (IHC) and immunofluorescence (IF), and comparison of TUNEL^{+} cells between the anti–colony-stimulating factor 1 receptor Ab (αCSF1R (continued)

complement activation than that of KiMs (Figure 5b–e). The differences in KRM signature gene scores at baseline (i.e., before αCSF1R Ab administration) were maintained after depletion and subsequent replication of KRMs (Figure 5f). However, identifying a phagocytosis-related signature specific to KRMs was challenging when using highly ranked genes. The expression of phagocytosis-related genes did not differ between KRMs and KiMs (Figure 5g), whereas the expression of efferocytosis-related genes was greater in KRMs than in KiMs (Figure 5h and i). Notably, among the efferocytosis-related genes, *Axl* was almost not expressed in KiMs or other immune cells. The protein expression of AXL was also greater in KRMs than in KiMs (Figure 5j). *In vitro* experiments revealed that $Axl^{-/-}$ KRMs had a lower capacity for efferocytosis than $Axl^{+/+}$ KRMs did (Figure 5k). At 24 weeks of age, AXL-depleted mice presented higher numbers of apoptotic cells, along with increased p53 expression and tubular damage, than wild-type mice (Figure 5l–n). Collectively, the deteriorative changes observed in the tubules of KRM-free kidneys may be attributable to the accumulation of apoptotic debris resulting from the absence of the KRM-specific efferocytotic function. In this process, the KRM-specific AXL molecule plays a role.

Suppression of $CD8^+$ T-cell activity by KRMs

We next investigated the impact of KRMs on other immune cells in noninjured, normal kidneys, focusing on both quantitative and qualitative aspects. With respect to quantitative changes, we examined the frequency of immune cells that underwent the most significant changes in the absence of KRMs. In the scRNA sequencing data set, a corresponding increase in NK cells was observed, as the number of KRMs was lower in the αCSF1R Ab–treated kidneys than in the control Ab-treated kidneys (Figure 6a). Flow cytometry analysis further confirmed an increase in both the number and frequency of NK cells in the αCSF1R Ab–treated kidneys (Figure 6b and Supplementary Figure S5 for the extended KRM-depleted condition). The proportions of NK cell subsets, based on CD11b and CD27 expression,[46] the frequency of the $CD49\alpha^+$ resident subset,[47] and cytokine production did not differ between αCSF1R Ab–treated and control Ab-treated kidneys (Figure 6c–e). The parenchymal expression of adhesion molecules for infiltrating NK cells remained unchanged between the 2 groups (Supplementary Figure S6). In terms of qualitative changes, the incoming and outgoing interactions among immune cells, referring respectively to the signals that cells receive from other cell types and the signals that they send out, were compared between the αCSF1R Ab–treated and control Ab-treated kidneys using the scRNA sequencing data set. Effector $CD8^+$ T cells were found to be most influenced by the absence of KRMs (Figure 6f and g). The upregulated pathways in effector $CD8^+$ T cells from αCSF1R Ab–treated kidneys were related to cellular morphology and protein production (Figure 6h). Analysis of the changes in transcription factors associated with effector $CD8^+$ T cells revealed increased expression patterns of *Junb*, *Crem*, *Klf6*, and *Nr4a1* in the αCSF1R Ab–treated kidneys (Figure 6i), which are linked to an inflammatory or activated T-cell phenotype.[48–50] Collectively, the absence of KRMs led to quantitative changes in NK cells and qualitative changes in effector $CD8^+$ T cells, highlighting the distinct roles that KRMs play in regulating these immune cell subsets.

We hypothesized that the effector $CD8^+$ T-cell subset, which exhibited the most significant qualitative changes in the absence of KRMs, is responsible for NK cell infiltration. To test this hypothesis, we examined the effects of combinations of chemokine ligands and receptors on these immune cells. The prominent chemokine receptor gene expressed by NK cells was *Ccr5*, followed by *Ccr2* (Figure 7a). Among the ligand genes for *Ccr5*, effector $CD8^+$ T cells primarily expressed the *Ccl5* gene (Figure 7b), which is consistent with findings from a previous study.[51] The production of CCL5 protein in $CD44^+$ $CD8^+$ T cells (corresponding to the effector $CD8^+$ T-cell subset) was greater in the αCSF1R Ab–treated group than in the control Ab-treated group (Figure 7c). Elevated gene transcription and protein production of CCL5 were also observed in overall kidney tissues (Figure 7d and e and Supplementary Figure S7 for analyses on day 63 and in the extended KRM-depleted condition). We confirmed the increased CCL5 production from $CD44^+$ $CD8^+$ T cells when $CD8^+$ T cells were

Figure 5 | (continued) Ab)– and control Ab-treated groups (n = 5 per group). The number of $TUNEL^+$ cells was calculated from the IHC images. Bars = 50 μm (IHC) and 100 μm (IF). (**b**) Uniform Manifold Approximation and Projection (UMAP) plots of 13,222 immune cells on day 42 after αCSF1R Ab or control Ab injection. (**c**) Dot plots to identify clusters. (**d**) Volcano plot showing gene expression fold changes between KRMs and kidney-infiltrating macrophages (KiMs). The genes showing the most significant changes are listed in the box. (**e**) Gene set enrichment analysis of Gene Ontology terms in order of normalized enrichment score (ES). (**f**) Scores of KRM-related genes before and 42 days after αCSF1R Ab injection. (**g**) Scores of phagocytosis-related genes in kidney macrophage subsets. (**h**) Dot plot showing efferocytosis-related genes. (**i**) Scores of efferocytosis-related genes in kidney macrophage subsets. (**j**) Representative flow cytometry plot of AXL expression in kidney macrophage subsets, and comparison of AXL^+ cells between 2 macrophage subsets on day 42 after Ab injection (n = 3 per group). No difference was detected between the αCSF1R Ab– and control Ab-treated groups. (**k**) *In vitro* efferocytotic capacity in single-cell suspension assay with apoptotic cells. (**l**) Comparison of $TUNEL^+$ cells in 24-week-old $Axl^{+/+}$ and $Axl^{-/-}$ mice (n = 5 per group). (**m**) Representative images of kidney sections from 24-week-old mice immunostained for p53, and comparison of the $p53^+$ area between $Axl^{+/+}$ and $Axl^{-/-}$ mice. (**n**) Comparison of tubular $KIM\text{-}1^+$ area in 24-week-old $Axl^{+/+}$ and $Axl^{-/-}$ mice. $^*P < 0.05$, $^{**}P < 0.01$, $^{***}P < 0.001$. cDC, classic dendritic cell; ILC, innate lymphoid cell; NK, natural killer; NKT, natural killer T; Nϕ, neutrophil; PC, plasma cell; T_{RM}, resident memory T. To optimize viewing of this image, please see the online version of this article at www.kidney-international.org.

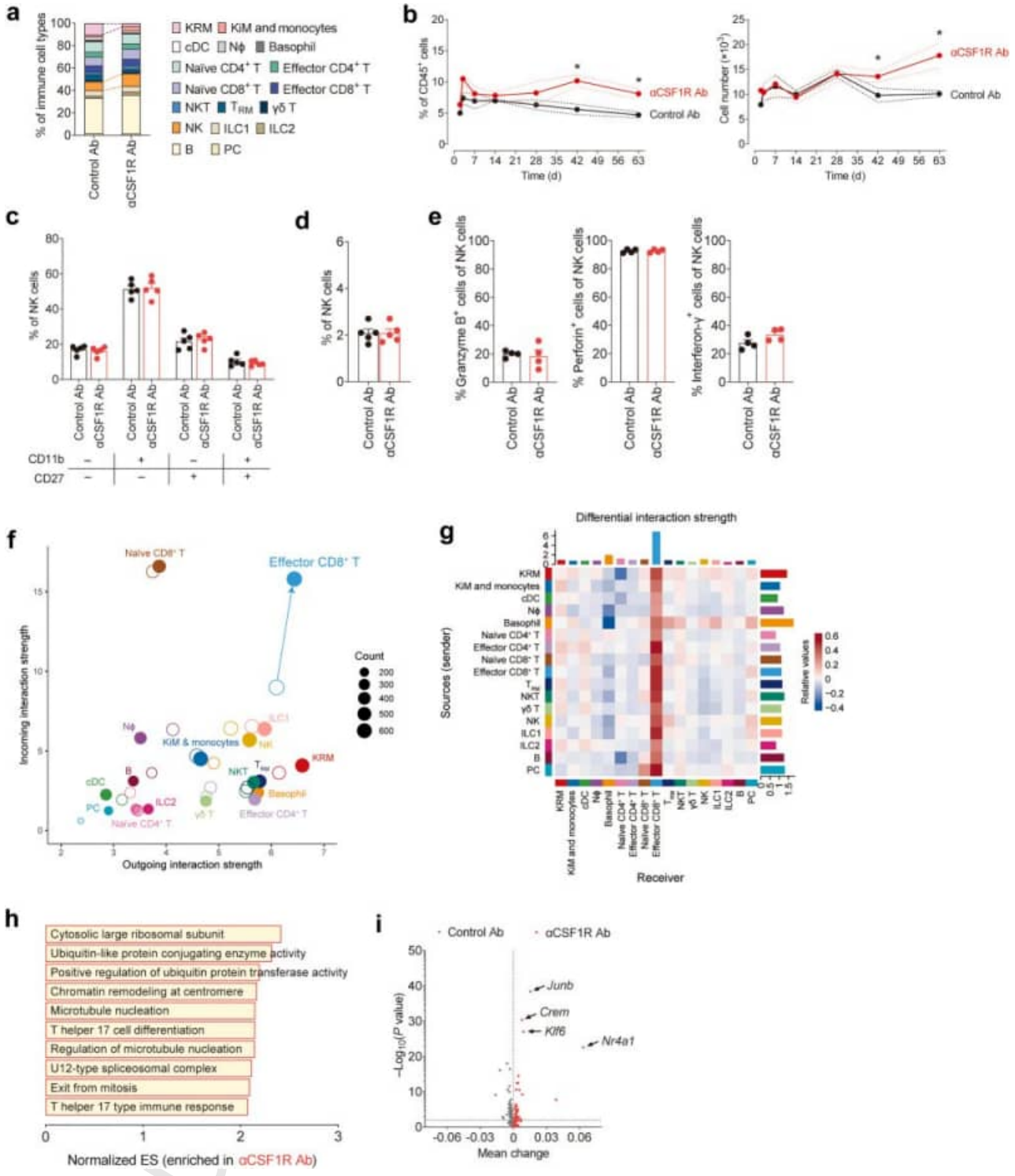

Figure 6 | Changes in immune cell subsets during the kidney-resident macrophages (KRM)–absent period. (**a**) Proportion of immune cell subsets on day 42 after antibody (Ab) injection. The calculations were derived from single-cell RNA sequencing data. (**b**) Flow cytometric analysis of the proportion (left) and cell number (right) of natural killer (NK) cells after Ab injection (n = 5∼6 per time point). (**c**) Proportion of NK cell subsets based on the expression of CD11b and CD27 on day 42 after Ab injection (n = 5 per group). (**d**) Proportion of CD49α^{+} resident NK cell subset (n = 5 per group). (**e**) Proportion of cytokine production in NK cells (n = 4 per group). (**f**) CellChat analysis results to identify cell-cell interactions on day 42 after Ab injection. The open and closed circles represent the control Ab- and anti–colony-stimulating factor 1 receptor Ab (αCSF1R Ab)–treated groups, respectively. (**g**) Heat map of differential interaction strengths. The red and blue color bars indicate an increase and decrease in interaction strength, respectively, in the αCSF1R Ab–treated group compared with the control Ab-treated group. The top and right colored bar plots denote the sum of incoming and outgoing signals in each cell cluster, respectively. (**h**) Gene set enrichment analysis of Gene Ontology terms in order of normalized enrichment score (ES) in the effector CD8^{+} T-cell cluster of (continued)

adoptively transferred into αCSF1R Ab–treated *Rag1*$^{-/-}$ mice compared with control Ab-treated mice (Figure 7f). These results suggest that, compared with the condition harboring KRMs, KiMs alone are insufficient to suppress CCL5 production from CD8^{+} T cells, highlighting the distinct role of KRMs in this regulatory process.

We examined the immune checkpoint molecules of KRMs and KiMs to determine whether their differential expression is responsible for altered crosstalk with CD8^{+} T cells and subsequent CCL5 production.[52–54] Among the genes encoding checkpoint molecules that provide negative signals to T cells, KRMs presented higher expression levels of *Vsir*, *Lgals9*, and *Cd200* than KiMs did, with *Vsir* showing the most significant difference between the 2 macrophage subsets (Figure 7g). VISTA (the protein encoded by the *Vsir* gene) is highly expressed in KRMs and plays a role in mitigating the inflammatory milieu after glomerular and tubular injuries.[13,15] We hypothesized that the overproduction of CCL5 in the absence of KRMs may be attributable to the low expression of VISTA in KiMs, resulting in reduced inhibitory signals to counterpart effector CD8^{+} T cells, as shown in previous study focused on cancer conditions.[55] These CD8^{+} T cells, as well as other T cells, expressed leucine-rich repeats and immunoglobulin-like domains 1 as a receptor for VISTA (Figure 7h).[56] Consistent with this hypothesis, CD44^{+} CD8^{+} T cells from *Vsir*$^{-/-}$ mice produced more CCL5 than those from *Vsir*$^{+/+}$ mice did (Figure 7i). Overall CCL5 production in kidney tissues was higher in *Vsir*$^{-/-}$ kidneys than in *Vsir*$^{+/+}$ kidneys (Figure 7j). This VISTA-dependent regulation of CCL5 production was also observed in an *in vitro* experiment where T-cell proliferation was assessed on VISTA-Fc–coated or control-Fc–coated plates (Figure 7k). Additionally, the frequency of NK cell infiltration was higher in *Vsir*$^{-/-}$ kidneys than in *Vsir*$^{+/+}$ kidneys (Figure 7l). Overall, in noninjured, normal kidneys, KRMs may maintain immunologic homeostasis through crosstalk with CD8^{+} T cells, with VISTA playing a key role in suppressing the overproduction of CCL5 and regulating NK cell infiltration within the kidneys.

Exacerbated tubulointerstitial nephritis in KRM-depleted kidneys

Despite the absence of KRMs, kidney function markers at the macro level were not altered (Figure 4f), but subcellular markers in both tubules and circulating immune cells notably changed. We then investigated the potential risk of toxin-induced AKI progression in KRM-deficient kidneys.[57,58] At the post–αCSF1R Ab or post–control Ab time points, we induced AKI with an adenine-mixed diet as the toxin. We established 2 time points for observation, days 42 and 63. On day 42, KRMs were entirely absent, whereas by day 63, they had been partially restored; nonetheless, immunologic changes persisted, including increased production of CCL5 and subsequent infiltration of NK cells (Figure 6b and Supplementary Figure S7). The disease progression was more rapid in the αCSF1R Ab–treated kidneys (i.e., KRM deficient or lacking) than in the control Ab-treated kidneys. This was evident in macrolevel changes, such as elevated blood urea nitrogen and serum creatinine levels (Figure 8a). The deposition of fibrotic materials was more severe in the αCSF1R Ab–treated kidneys than in the control Ab-treated kidneys (Figure 8b). When we applied a folic acid–induced injury model as an alternative AKI model,[59] the αCSF1R Ab–treated kidneys sustained higher damage than did the control Ab-treated kidneys (Supplementary Figure S8).

We next examined whether the course of toxin-induced AKI was altered in KRMs lacking the characteristic checkpoint molecules, AXL and VISTA. Compared with their wild-type counterparts, *Vsir*$^{-/-}$ mice exhibited severe injury following adenine-mixed diet, consistent with previous studies,[13,15] whereas *Axl* gene deletion was not associated with AKI progression but rather was protective when AXL was present (Figure 8c and d). The deposition of fibrotic material due to AKI was higher in *Vsir*$^{-/-}$ mice than in wild-type mice, whereas fibrosis in *Axl*$^{-/-}$ kidneys did not differ from that in *Axl*$^{+/+}$ kidneys (Figure 8e and f). The difference in the progression of toxin-induced AKI depending on the expression of the 2 molecules is likely due to the difference in expression patterns between AXL and VISTA during disease progression (Supplementary Figure S9). Specifically, VISTA was expressed primarily in macrophages even as disease progressed, whereas AXL was also expressed in glomerular and tubular parenchymal tissues, which supports the previous study results.[60]

Human translation of mouse results

To translate these findings from mouse models to humans, we analyzed kidney tissues from patients with biopsy-confirmed toxin-induced AKI. The baseline characteristics of these patients are presented in Supplementary Table 3. CD68^{+} mononuclear phagocytes (MNPs), including macrophages, were more widely distributed in the interstitial areas of AKI tissues than in noninjured tissues (Figure 9a). Given that macrophage heterogeneity influences the direction of TIN progression,[61] we sought to compare the distribution of KRM-like and KiM-like MNPs, as well as their levels of AXL and VISTA expression, in toxin-induced AKI. Using scRNA sequencing data sets of normal human kidneys,[62–66] we identified KRM-like and KiM-like MNP clusters based on the expression of *C1QC*, *APOE*, *CD163*, *CD74*, *HLA-DRA*, *FCN1*, *VCAN*, *IFITM2*, and *CDKN1C* (Figure 9c). Among parenchymal tissue cells, *AXL* gene expression was predominantly observed in podocytes,

Figure 6 | (continued) the αCSF1R Ab–treated group compared with the control Ab-treated group. (**i**) Volcano plot of differential transcription factors in effector CD8^{+} T cells between the αCSF1R Ab– and control Ab-treated groups. *$P < 0.05$. cDC, classic dendritic cell; ILC, innate lymphoid cell; KiM, kidney-infiltrating macrophage; NKT, natural killer T cell; Nϕ, neutrophil; PC, plasma cell; T_{RM}, resident memory T.

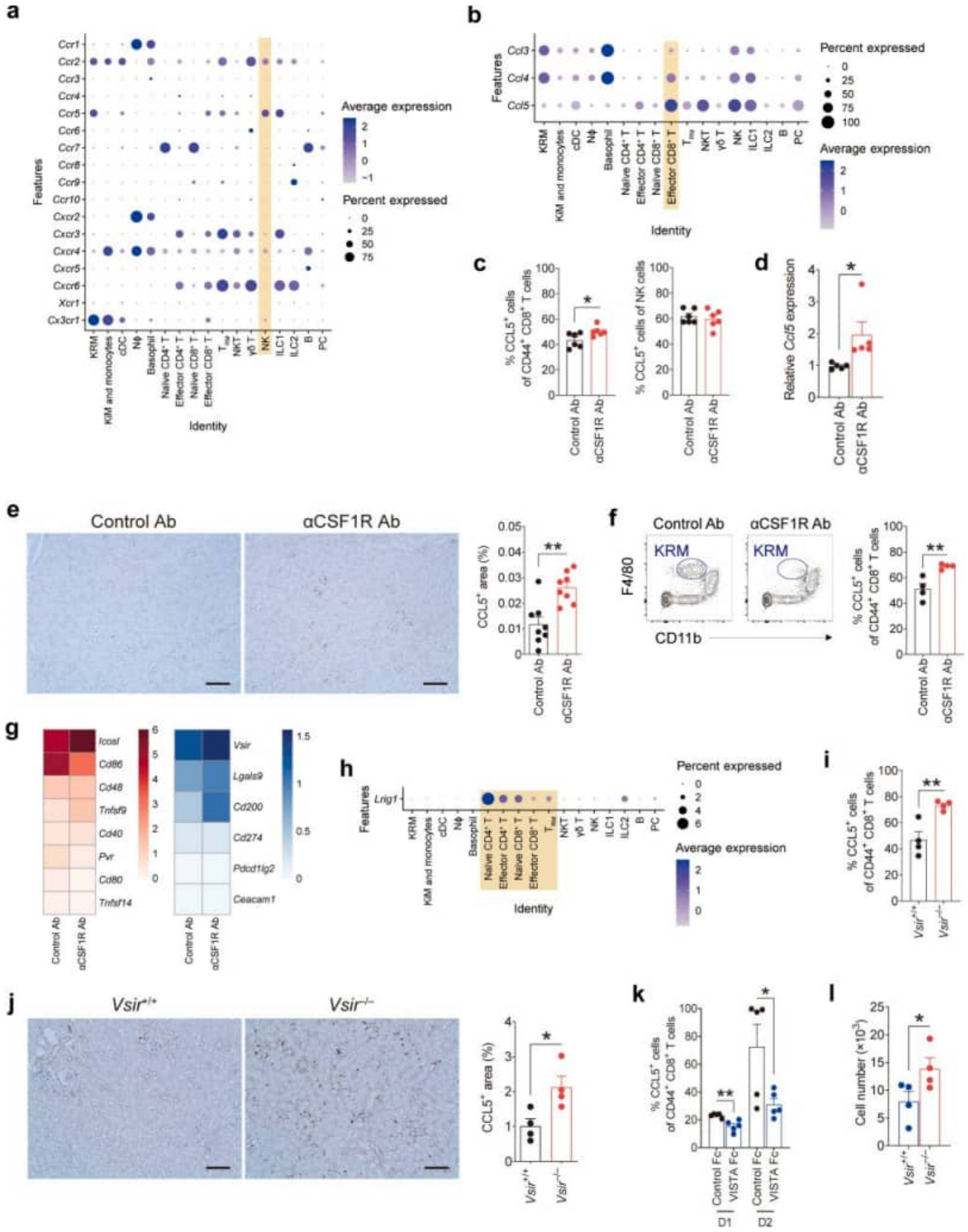

Figure 7 | Natural killer (NK) cell infiltration via crosstalk between kidney-resident macrophage (KRM) and effector CD8$^+$ T cells. (**a**) Dot plot to identify the gene expression of chemokine receptors in each cluster. Gene expression for the NK cluster is highlighted in yellow. (**b**) Dot plot to identify the gene expression of chemokine ligands in each cluster. Gene expression for the effector CD8$^+$ T-cell cluster is highlighted in yellow. (**c**) Flow cytometric analysis of C-C motif chemokine ligand 5 (CCL5) production in effector CD8$^+$ T cells (continued)

whereas the chromosome 10 open reading frame 54 (*C10orf54*; the human gene name for *Vsir*) gene was expressed in podocytes and endothelial cells (Figure 9d). Among *PTPRC*$^{+}$ immune cells, *AXL* gene expression was primarily found in KRM-like MNPs, whereas *C10orf54* gene expression was present in both KRM-like and KiM-like MNPs. Next, we aimed to validate the observed differences in *AXL* and *VISTA* gene expression at the protein level. Among the genes distinguishing KRM-like from KiM-like MNPs, we selected *VSIG4* as a marker with minimal expression in parenchymal tissues (Supplementary Figure S10). We then performed costaining for CD68 and VSIG4 in kidney tissues from patients with toxin-induced AKI (Figure 9e), and classified the cells as KRM-like MNPs (CD68^{+} VSIG4^{+}) and KiM-like MNPs (CD68^{+} VSIG4^{-}) accordingly. KRM-like MNPs exhibited high levels of AXL and VISTA protein expression, whereas KiM-like MNPs showed low expression of both markers (Figure 9F). On the basis of the proportion of KRMs among CD68^{+} MNPs, samples were divided into KRM-high and KRM-low groups to compare the risk of kidney disease progression following AKI. Accordingly, the group with a high KRM distribution tended to exhibit a lower risk of kidney disease progression than the group with a low KRM distribution (Figure 9g). These findings suggest that the presence of AXL^{+} and VISTA^{+} human KRMs, which correspond to mouse KRMs, may help maintain kidney homeostasis and provide individualized risk stratification for AKI progression following toxin-induced injury.

DISCUSSION

Although many studies have suggested the homeostatic role of KRMs, there has been no direct clue regarding their impact on surrounding parenchymal tissue and immune cells when KRMs are absent in noninjured kidneys. The present study addresses this gap by using a model of long-term KRM depletion using both cellular dynamics and αCSF1R Ab treatment. The CCL2-CCR2 axis and transcription factor machinery are involved in these cyclical periods of depletion and repletion. KRM-depleted kidneys harbor p53^{high} tubules with damage markers, which is attributable to the lack of efficient efferocytosis performed by AXL^{high} KRMs. Among the surrounding immune cells, effector CD8^{+} T cells displayed the most pronounced changes in the absence of KRMs, including increased CCL5 production and NK cell infiltration, which was linked to the VISTA molecule, which is highly expressed in KRMs. These alterations contributed to an increased risk of progression after toxin administration, a finding that was also observed in human cases of toxin-induced AKI. Therefore, maintaining a population of KRMs within the interstitial niche may help reduce the risk of AKI progression before such insults occur.

Nephrotoxic agents may provoke AKI by disrupting homeostasis.[67] However, this inflammatory event does not occur in everyone but is more likely in individuals with certain risk factors. Therefore, research on the immunologic status of noninjured baseline kidneys is critical because it can help predict individualized responses to such insults. In noninjured kidneys, KRMs constitute most resident immune cells,[6,12,13] and their infiltration into the interstitial niche appears to be dependent on the CCR2-CCL2 axis, consistent with previous findings.[18,30] Although KRMs inherently express molecules that can promote inflammation,[40] they are expected to play a role in regulating the inflammatory response.[13,15] The roles identified in the present study include highly efficient efferocytosis and the modulation of CD8^{+} T-cell activity through checkpoint molecules, such as AXL and VISTA, which likely reduce kidney stress before disease onset. Therefore, in clinical practice, the distribution of KRMs within the kidney or the expression levels of AXL and VISTA could serve as immunologic biomarkers to determine an individual's response to nephrotoxic agents.

The AXL molecule is a member of the TYRO3-AXL-MERTK receptor family.[68] This molecule has garnered particular attention in the field of cancer immunity because of its high expression in tumor cells, where it enables these cells to evade immune recognition and destruction.[69] Numerous therapeutic agents targeting AXL are currently under development for cancer treatment. However, AXL is also naturally expressed in various cell types, particularly in phagocytes, where it plays a crucial role in the clearance of apoptotic cells.[70] The absence of AXL expression is associated with tissue inflammation due to the accumulation of uncleared apoptotic debris.[71,72] In the kidney, AXL is more

Figure 7 | (continued) and NK cells on day (D) 42 after antibody (Ab) injection (n = 6 per group). (**d**) Expression of the *Ccl5* gene in kidneys from the anti–colony-stimulating factor 1 receptor Ab (αCSF1R Ab)– and control Ab-treated groups (n = 5 per group). (**e**) Representative images of kidney sections immunostained for CCL5 on day 42 after Ab injection, and comparison of the CCL5^{+} areas between the αCSF1R Ab– and control Ab-treated groups (n = 8 per group). (**f**) Representative flow cytometric plots on day 42 after Ab injection in *Rag1*$^{-/-}$ mice, and comparison of CCL5 production from adoptively transferred effector CD8^{+} cells between the αCSF1R Ab– and control Ab-treated groups (n = 4 per group). (**g**) Heat map showing the gene expression of immune checkpoint stimulatory (left) and inhibitory (right) molecules in KRMs compared with kidney-infiltrating macrophages (KiMs). Genes are listed in order of their expression levels in KRMs. (**h**) Dot plot to identify *Lrig1* gene expression in each cluster. (**i**) Flow cytometric analysis of CCL5 production in effector CD8^{+} T cells from the *Vsir*$^{+/+}$ and *Vsir*$^{-/-}$ kidneys of 6-month-old mice (n = 4 per group). (**j**) Representative images of kidney sections from 6-month-old mice immunostained for CCL5, and comparison of the CCL5^{+} area between *Vsir*$^{+/+}$ and *Vsir*$^{-/-}$ kidneys (n = 4 per group). (**k**) Flow cytometric analysis of CCL5 production from sorted effector CD8^{+} T cells on plates coated with anti-CD3 antibodies and either VISTA-Fc or control-Fc. (**l**) Comparison of the number of NK cells per kidney in 6-month-old *Vsir*$^{+/+}$ and *Vsir*$^{-/-}$ mice (n = 4 per group). *$P < 0.05$, **$P < 0.01$. cDC, classic dendritic cell; ILC, innate lymphoid cell; NKT, natural killer T cell; Nϕ, neutrophil; PC, plasma cell; T_{RM}, resident memory T; VISTA, V-domain immunoglobulin suppressor of T-cell activation. To optimize viewing of this image, please see the online version of this article at www.kidney-international.org.

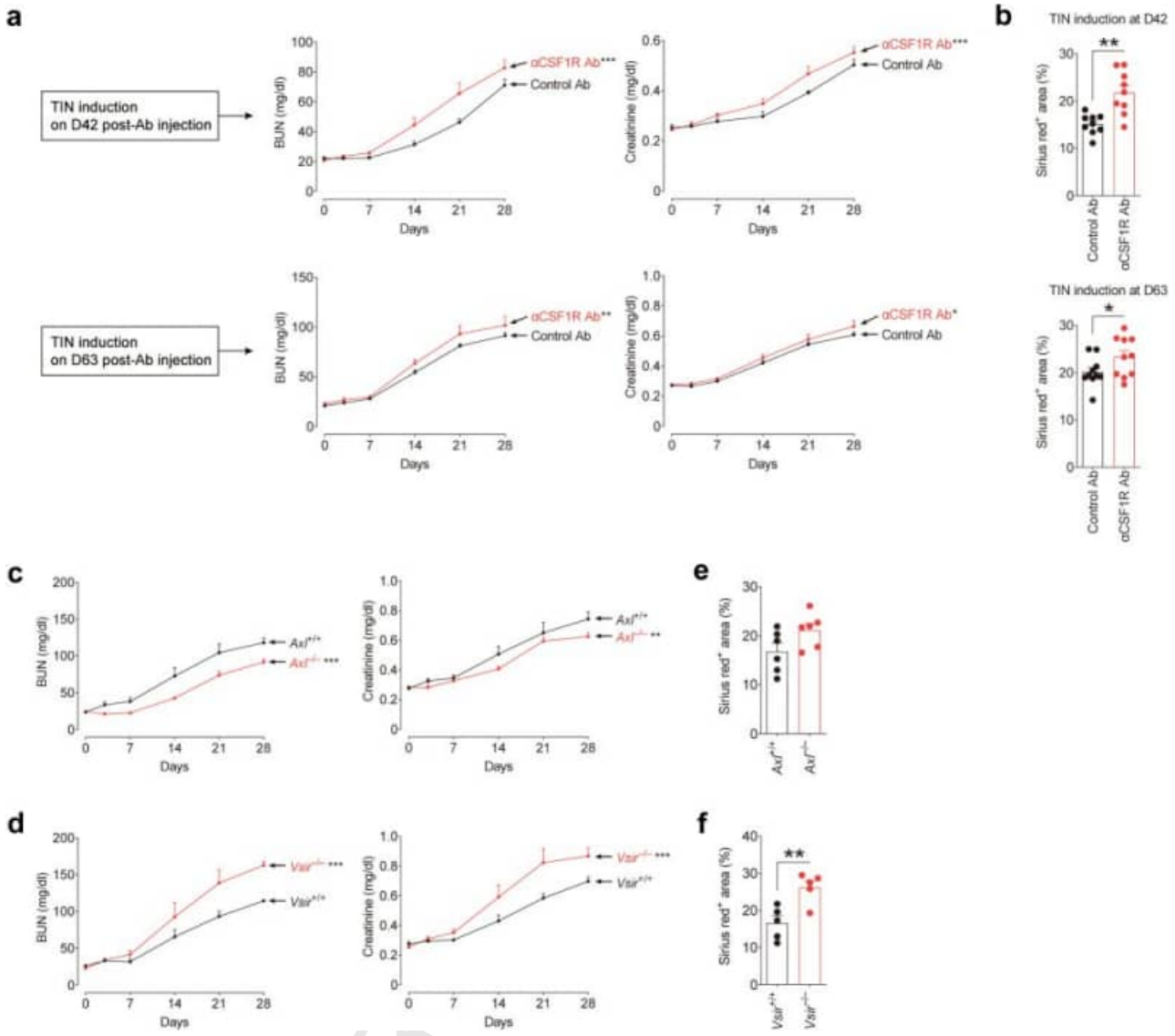

Figure 8 | Progression of toxin-induced acute kidney injury (AKI) according to the presence of kidney-resident macrophages or their signatures. (**a**) Tubular damage markers after AKI induction with adenine-mixed diet on day (D) 42 or 63 after antibody (Ab) injection (n = 9∼10 per group). (**b**) Comparison of kidney fibrosis on day 28 after AKI induction between anti–colony-stimulating factor 1 receptor Ab (αCSF1R Ab)–treated and control Ab-treated groups (n = 9∼10 per group). (**c**) Comparison of tubular damage markers between *Axl*$^{+/+}$ and *Axl*$^{-/-}$ kidneys after AKI induction with adenine-mixed diet (n = 6 per group). (**d**) Comparison of tubular damage markers between *Vsir*$^{+/+}$ and *Vsir*$^{-/-}$ kidneys after AKI induction with adenine-mixed diet (n = 5 per group). (**e**) Comparison of fibrosis between *Axl*$^{+/+}$ and *Axl*$^{-/-}$ kidneys on day 28 after AKI induction with adenine-mixed diet (n = 6 per group). (**f**) Comparison of fibrosis between *Vsir*$^{+/+}$ and *Vsir*$^{-/-}$ kidneys on day 28 after AKI induction with adenine-mixed diet (n = 5 per group). *$P < 0.05$, **$P < 0.01$, ***$P < 0.001$. BUN, blood urea nitrogen; TIN, tubulointerstitial nephritis.

highly expressed in KRMs than in KiMs or other immune cells, suggesting its role in KRM-dependent homeostatic surveillance through timely removal of cellular debris. However, AXL is also expressed in podocytes, and its expression is augmented in both glomerular and tubular cells under inflammatory conditions.[60] Owing to this expression pattern, *Axl*-deficient mice did not undergo overzealous progression of TIN. When an AXL-targeting inhibitor was used in the glomerular injury model, glomerulonephritis was alleviated.[73] Therefore, rather than using AXL enhancers or inhibitors that target the entire kidney, developing agents that specifically target KRMs or KiMs for immunologic maintenance under noninjured conditions may be more effective.

VISTA is an immunoregulatory and inhibitory checkpoint molecule expressed in cells of both the myeloid and lymphoid lineages.[74] In the context of cancer, VISTA^{high} macrophages deliver negative signals to T cells, thereby promoting cancer progression.[75–77] In noninjured kidneys, KRMs naturally and highly express VISTA, and their residency helps mitigate the immunofibrotic processes following tubular or glomerular injury.[13,15] We further explored the

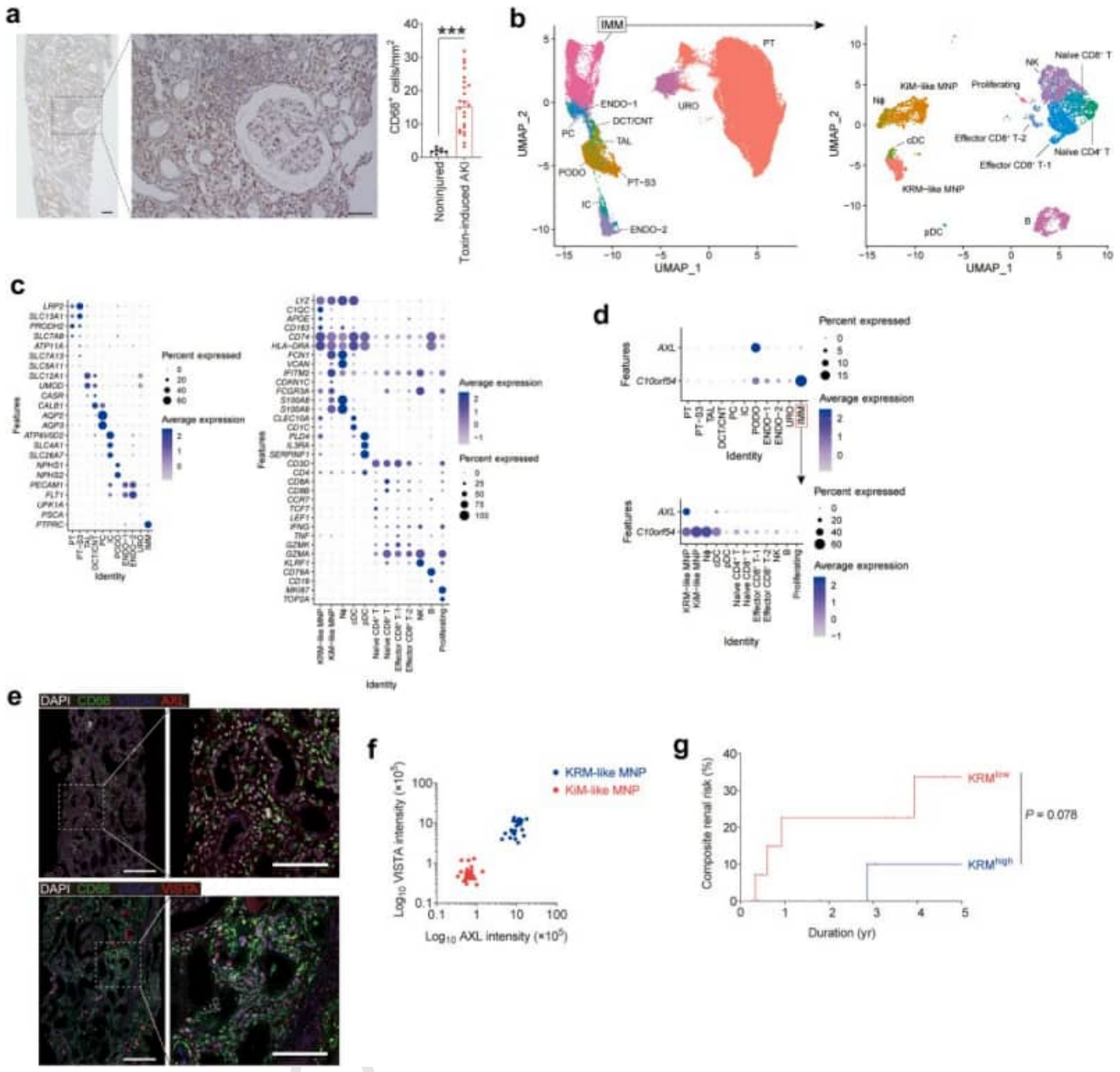

Figure 9 | Translation of the results to human samples. (**a**) Representative image of kidney sections immunostained for CD68 in a patient with toxin-induced acute kidney injury (AKI), and comparison of the number of $CD68^+$ cells between noninjured (n = 7) and AKI (n = 27) kidneys. Bars = 100 μm. (**b**) Uniform Manifold Approximation and Projection (UMAP) plots of 92,511 kidney cells from 31 healthy humans. (**c**) Dot plots to identify clusters of parenchymal tissue cells (left) and immune cells (right). (**d**) Dot plots to identify the *AXL* and *C10orf54* gene expression in each cluster. (**e**) Representative images of kidney tissues from patients with toxin-induced AKI, immunostained for 4′,6-diamidino-2-phenylindole (DAPI), CD68, VSIG4, and AXL (top) or V-domain immunoglobulin suppressor of T-cell activation (VISTA) (bottom). Bars = 200 μm (left) and 100 μm (right). (**f**) Expression patterns of AXL and VISTA in kidney-resident macrophage (KRM)–like and kidney-infiltrating macrophage (KiM)–like mononuclear phagocytes (MNPs). (**g**) Kidney disease progression in patients with toxin-induced AKI, stratified by KRM^{high} and KRM^{low} fractions within MNPs. ***$P < 0.001$. cDC, classic dendritic cell; CNT, connecting tubule; DCT, distal convoluted tubule; ENDO, endothelium; IC, intercalated cell of collecting duct; IMM, immune cell; NK, natural killer; T; Nϕ, neutrophil; PC, principal cell of collecting duct; PODO, podocyte; PT, proximal tubule; PT-S3, segment 3 of proximal tubule; TAL, thick ascending limb; URO, urothelial cell. To optimize viewing of this image, please see the online version of this article at www.kidney-international.org.

interaction between KRMs and effector $CD8^+$ T cells in noninjured kidneys. CCL5 expression in effector $CD8^+$ T cells was influenced by $VISTA^{high}$ KRMs, leading to NK cell infiltration and increased susceptibility to TIN. However, it is still unknown which signaling pathway via VISTA modulates CCL5 expression in these T cells under noninjured conditions. Further research is required to elucidate the related signaling pathways.

In conclusion, the present study provides the first evidence that KRMs play a crucial role in maintaining

FLA 5.7.0 DTD ■ KINT4344_proof ■ 4 September 2025 ■ ce

homeostasis in noninjured kidneys, owing to their hallmark function and molecular signatures compared with those of KiMs. Understanding the cellular dynamics of heterogeneous macrophages during rhythmic cycles of depletion and repletion will be instrumental in developing strategies to preserve immunologic homeostasis. Additionally, these findings offer valuable insights into the prevention of toxin-induced AKI and suggest the potential use of macrophage-specific biomarkers to individualize the assessment of disease risk.

DISCLOSURE

All the authors declared no competing interests.

DATA STATEMENT

The single-cell RNA (scRNA) sequencing data sets for sorted CD11b^{+} cells (after anti–colony-stimulating factor 1 receptor antibody [αCSF1R Ab] use), sorted CD45^{+} cells, and total kidney cells (after the use of αCSF1R Ab or control Ab) have been deposited in the Gene Expression Omnibus database (accession numbers: GSE273341 and GSE294497). The scRNA sequencing data sets for human kidneys are available from the Kidney Cell Atlas (https://www.kidneycellatlas.org/) and the Gene Expression Omnibus database (accession numbers: GSM3689774, GSE134355, GSE131685, and GSE202109). This study does not provide any original code, and the codes used are accessible in the Methods section. Any further information required to reanalyze the data is available from the lead contact on request.

ACKNOWLEDGMENTS

This work was supported by the National Research Foundation (NRF) of Korea (NRF-2023R1A2C1005753 to SSH) and the Korea Health Technology R&D project through the Korea Health Industry Development Institute (RS-2024-00406325 to SSH). Human biospecimens were provided by the Biobank of Seoul National University Hospital, a member of the Korea Biobank Network (KBN4_A03), which is supported by the Korea Centers for Disease Control and Prevention (number 4845-303). This research used core resources of the Center for Medical Innovation of Seoul National University Hospital.

AUTHOR CONTRIBUTIONS

SSH, MH, and DY designed the study. MH, JH, CK, HY, S-KS, BJ, and JO performed experiments and analyzed data. DY, PGP, HMS, and DKK analyzed bioinformatics data. KCM and SSH supervised histology studies. DKK, K-HO, and KWJ collected data. D-SL, YSK, and SSH interpreted data and provided critical reading of the manuscript. MH, DY, and SSH wrote the manuscript. All of the authors approved the final manuscript.

Supplementary material is available online at www.kidney-international.org.

REFERENCES

1. Praga M, González E. Acute interstitial nephritis. *Kidney Int*. 2010;77:956–961.
2. Baker RJ, Pusey CD. The changing profile of acute tubulointerstitial nephritis. *Nephrol Dial Transplant*. 2004;19:8–11.
3. Yun D, Jang MJ, An JN, et al. Effect of steroids and relevant cytokine analysis in acute tubulointerstitial nephritis. *BMC Nephrol*. 2019;20:88.
4. Perazella MA, Shirali AC. Immune checkpoint inhibitor nephrotoxicity: what do we know and what should we do? *Kidney Int*. 2020;97:62–74.
5. Wu IW, Wu YL, Yang HY, et al. Deep immune profiling of patients with renal impairment unveils distinct immunotypes associated with disease severity. *Clin Kidney J*. 2023;16:78–89.
6. Park JG, Na M, Kim MG, et al. Immune cell composition in normal human kidneys. *Sci Rep*. 2020;10:15678.
7. Clarkson MR, Giblin L, O'Connell FP, et al. Acute interstitial nephritis: clinical features and response to corticosteroid therapy. *Nephrol Dial Transplant*. 2004;19:2778–2783.
8. Muriithi AK, Leung N, Valeri AM, et al. Biopsy-proven acute interstitial nephritis, 1993-2011: a case series. *Am J Kidney Dis*. 2014;64:558–566.
9. Blériot C, Chakarov S, Ginhoux F. tissue Determinants of resident tissue macrophage identity and function. *Immunity*. 2020;52:957–970.
10. Szabo PA, Miron M, Farber DL. Location, location, location: tissue resident memory T cells in mice and humans. *Sci Immunol*. 2019;4:eaas9673.
11. Davies LC, Jenkins SJ, Allen JE, et al. Tissue-resident macrophages. *Nat Immunol*. 2013;14:986–995.
12. Cheung MD, Agarwal A, George JF. Where are they now: spatial and molecular diversity of tissue-resident macrophages in the kidney. *Semin Nephrol*. 2022;42:151276.
13. Park JG, Lee CR, Kim MG, et al. Kidney residency of VISTA-positive macrophages accelerates repair from ischemic injury. *Kidney Int*. 2020;97:980–994.
14. Cao Q, Wang Y, Wang XM, et al. Renal F4/80+ CD11c+ mononuclear phagocytes display phenotypic and functional characteristics of macrophages in health and in adriamycin nephropathy. *J Am Soc Nephrol*. 2015;26:349–363.
15. Kim MG, Yun D, Kang CL, et al. Kidney VISTA prevents IFN-γ/IL-9 axis-mediated tubulointerstitial fibrosis after acute glomerular injury. *J Clin Invest*. 2022;132:e151189.
16. Nelson PJ, Rees AJ, Griffin MD, et al. The renal mononuclear phagocytic system. *J Am Soc Nephrol*. 2012;23:194–203.
17. Cao Q, Harris DC, Wang Y. Macrophages in kidney injury, inflammation, and fibrosis. *Physiology (Bethesda)*. 2015;30:183–194.
18. Stamatiades EG, Tremblay ME, Bohm M, et al. Immune monitoring of trans-endothelial transport by kidney-resident macrophages. *Cell*. 2016;166:991–1003.
19. He J, Cao Y, Zhu Q, et al. Renal macrophages monitor and remove particles from urine to prevent tubule obstruction. *Immunity*. 2024;57:106–123.e107.
20. Liu Z, Gu Y, Chakarov S, et al. Fate mapping via Ms4a3-expression history traces monocyte-derived cells. *Cell*. 2019;178:1509–1525.e1519.
21. Mass E, Nimmerjahn F, Kierdorf K, et al. Tissue-specific macrophages: how they develop and choreograph tissue biology. *Nat Rev Immunol*. 2023;23:563–579.
22. Hagemeyer N, Kierdorf K, Frenzel K, et al. Transcriptome-based profiling of yolk sac-derived macrophages reveals a role for Irf8 in macrophage maturation. *EMBO J*. 2016;35:1730–1744.
23. Zimmerman KA, Yang Z, Lever JM, et al. Kidney resident macrophages in the rat have minimal turnover and replacement by blood monocytes. *Am J Physiol Renal Physiol*. 2021;321:F162–F169.
24. Zhu Q, Xiao L, Cheng G, et al. Self-maintaining macrophages within the kidney contribute to salt and water balance by modulating kidney sympathetic nerve activity. *Kidney Int*. 2023;104:324–333.
25. Nash WT, Yee MS, Okusa MD. Myeloid response to acute kidney injury. *Nephron*. 2023;147:39–43.
26. MacDonald KP, Palmer JS, Cronau S, et al. An antibody against the colony-stimulating factor 1 receptor depletes the resident subset of monocytes and tissue- and tumor-associated macrophages but does not inhibit inflammation. *Blood*. 2010;116:3955–3963.
27. Lemley KV, Kriz W. Anatomy of the renal interstitium. *Kidney Int*. 1991;39:370–381.
28. Cheung MD, Erman EN, Moore KH, et al. Resident macrophage subpopulations occupy distinct microenvironments in the kidney. *JCI Insight*. 2022;7:e161078.
29. Wang X, Chen J, Xu J, et al. The role of macrophages in kidney fibrosis. *Front Physiol*. 2021;12:705838.
30. Li L, Huang L, Sung SS, et al. The chemokine receptors CCR2 and CX3CR1 mediate monocyte/macrophage trafficking in kidney ischemia-reperfusion injury. *Kidney Int*. 2008;74:1526–1537.
31. Dick SA, Wong A, Hamidzada H, et al. Three tissue resident macrophage subsets coexist across organs with conserved origins and life cycles. *Sci Immunol*. 2022;7:eabf7777.

32. Bajpai G, Bredemeyer A, Li W, et al. Tissue resident CCR2- and CCR2+ cardiac macrophages differentially orchestrate monocyte recruitment and fate specification following myocardial injury. *Circ Res*. 2019;124:263–278.
33. Geissmann F, Jung S, Littman DR. Blood monocytes consist of two principal subsets with distinct migratory properties. *Immunity*. 2003;19:71–82.
34. Anders HJ, Vielhauer V, Schlöndorff D. Chemokines and chemokine receptors are involved in the resolution or progression of renal disease. *Kidney Int*. 2003;63:401–415.
35. T'Jonck W, Guilliams M, Bonnardel J. Niche signals and transcription factors involved in tissue-resident macrophage development. *Cell Immunol*. 2018;330:43–53.
36. Lavin Y, Winter D, Blecher-Gonen R, et al. Tissue-resident macrophage enhancer landscapes are shaped by the local microenvironment. *Cell*. 2014;159:1312–1326.
37. Schulz C, Gomez Perdiguero E, Chorro L, et al. A lineage of myeloid cells independent of Myb and hematopoietic stem cells. *Science*. 2012;336:86–90.
38. Guilliams M, Svedberg FR. Does tissue imprinting restrict macrophage plasticity? *Nat Immunol*. 2021;22:118–127.
39. Jenkins SJ, Allen JE. The expanding world of tissue-resident macrophages. *Eur J Immunol*. 2021;51:1882–1896.
40. Lever JM, Hull TD, Boddu R, et al. Resident macrophages reprogram toward a developmental state after acute kidney injury. *JCI Insight*. 2019;4:e125503.
41. Gaynor R, Simon K, Koeffler P. Expression of c-jun during macrophage differentiation of HL-60 cells. *Blood*. 1991;77:2618–2623.
42. Liu H, Shi B, Huang CC, et al. Transcriptional diversity during monocyte to macrophage differentiation. *Immunol Lett*. 2008;117:70–80.
43. Carter JH, Tourtellotte WG. Early growth response transcriptional regulators are dispensable for macrophage differentiation. *J Immunol*. 2007;178:3038–3047.
44. Megyesi J, Safirstein RL, Price PM. Induction of p21WAF1/CIP1/SDI1 in kidney tubule cells affects the course of cisplatin-induced acute renal failure. *J Clin Invest*. 1998;101:777–782.
45. Ying Y, Kim J, Westphal SN, et al. Targeted deletion of p53 in the proximal tubule prevents ischemic renal injury. *J Am Soc Nephrol*. 2014;25:2707–2716.
46. Chiossone L, Chaix J, Fuseri N, et al. Maturation of mouse NK cells is a 4-stage developmental program. *Blood*. 2009;113:5488–5496.
47. Victorino F, Sojka DK, Brodsky KS, et al. Tissue-resident NK cells mediate ischemic kidney injury and are not depleted by anti-Asialo-GM1 antibody. *J Immunol*. 2015;195:4973–4985.
48. Riera-Sans L, Behrens A. Regulation of alphabeta/gammadelta T cell development by the activator protein 1 transcription factor c-Jun. *J Immunol*. 2007;178:5690–5700.
49. Cao Z, Sun X, Icli B, et al. Role of Kruppel-like factors in leukocyte development, function, and disease. *Blood*. 2010;116:4404–4414.
50. Best JA, Blair DA, Knell J, et al. Transcriptional insights into the CD8(+) T cell response to infection and memory T cell formation. *Nat Immunol*. 2013;14:404–412.
51. Schall TJ, Bacon K, Toy KJ, et al. Selective attraction of monocytes and T lymphocytes of the memory phenotype by cytokine RANTES. *Nature*. 1990;347:669–671.
52. Wykes MN, Lewin SR. Immune checkpoint blockade in infectious diseases. *Nat Rev Immunol*. 2018;18:91–104.
53. Chen L, Flies DB. Molecular mechanisms of T cell co-stimulation and co-inhibition. *Nat Rev Immunol*. 2013;13:227–242.
54. Mantovani A, Allavena P, Marchesi F, et al. Macrophages as tools and targets in cancer therapy. *Nat Rev Drug Discov*. 2022;21:799–820.
55. Broughton TWK, ElTanbouly MA, Schaafsma E, et al. Defining the signature of VISTA on myeloid cell chemokine responsiveness. *Front Immunol*. 2019;10:2641.
56. Ta HM, Roy D, Zhang K, et al. LRIG1 engages ligand VISTA and impairs tumor-specific CD8(+) T cell responses. *Sci Immunol*. 2024;9:eadi7418.
57. Yokozawa T, Zheng PD, Oura H, et al. Animal model of adenine-induced chronic renal failure in rats. *Nephron*. 1986;44:230–234.
58. Kang C, Yun D, Yoon H, et al. Glutamyl-prolyl-tRNA synthetase (EPRS1) drives tubulointerstitial nephritis-induced fibrosis by enhancing T cell proliferation and activity. *Kidney Int*. 2024;105:997–1019.
59. Fink M, Henry M, Tange JD. Experimental folic acid nephropathy. *Pathology*. 1987;19:143–149.
60. Fiebeler A, Park JK, Muller DN, et al. Growth arrest specific protein 6/Axl signaling in human inflammatory renal diseases. *Am J Kidney Dis*. 2004;43:286–295.
61. Wen Y, Yan HR, Wang B, et al. Macrophage heterogeneity in kidney injury and fibrosis. *Front Immunol*. 2021;12:681748.
62. Zimmerman KA, Bentley MR, Lever JM, et al. Single-cell RNA sequencing identifies candidate renal resident macrophage gene expression signatures across species. *J Am Soc Nephrol*. 2019;30:767–781.
63. Liao J, Yu Z, Chen Y, et al. Single-cell RNA sequencing of human kidney. *Sci Data*. 2020;7:4.
64. Han X, Zhou Z, Fei L, et al. Construction of a human cell landscape at single-cell level. *Nature*. 2020;581:303–309.
65. Stewart BJ, Ferdinand JR, Young MD, et al. Spatiotemporal immune zonation of the human kidney. *Science*. 2019;365:1461–1466.
66. McEvoy CM, Murphy JM, Zhang L, et al. Single-cell profiling of healthy human kidney reveals features of sex-based transcriptional programs and tissue-specific immunity. *Nat Commun*. 2022;13:7634.
67. Gérard AO, Merino D, Laurain A, et al. Drug-induced tubulointerstitial nephritis: insights from the World Health Organization safety database. *Kidney Int Rep*. 2022;7:1699–1702.
68. Liu E, Hjelle B, Bishop JM. Transforming genes in chronic myelogenous leukemia. *Proc Natl Acad Sci U S A*. 1988;85:1952–1956.
69. Zhu C, Wei Y, Wei X. AXL receptor tyrosine kinase as a promising anti-cancer approach: functions, molecular mechanisms and clinical applications. *Mol Cancer*. 2019;18:153.
70. Seitz HM, Camenisch TD, Lemke G, et al. Macrophages and dendritic cells use different Axl/Mertk/Tyro3 receptors in clearance of apoptotic cells. *J Immunol*. 2007;178:5635–5642.
71. van der Meer JH, van der Poll T, van 't Veer C. TAM receptors, Gas6, and protein S: roles in inflammation and hemostasis. *Blood*. 2014;123:2460–2469.
72. Weinger JG, Brosnan CF, Loudig O, et al. Loss of the receptor tyrosine kinase Axl leads to enhanced inflammation in the CNS and delayed removal of myelin debris during experimental autoimmune encephalomyelitis. *J Neuroinflammation*. 2011;8:49.
73. Zhen Y, Lee IJ, Finkelman FD, et al. Targeted inhibition of Axl receptor tyrosine kinase ameliorates anti-GBM-induced lupus-like nephritis. *J Autoimmun*. 2018;93:37–44.
74. ElTanbouly MA, Schaafsma E, Noelle RJ, et al. VISTA: coming of age as a multi-lineage immune checkpoint. *Clin Exp Immunol*. 2020;200:120–130.
75. Wang L, Rubinstein R, Lines JL, et al. VISTA, a novel mouse Ig superfamily ligand that negatively regulates T cell responses. *J Exp Med*. 2011;208:577–592.
76. Gao J, Ward JF, Pettaway CA, et al. VISTA is an inhibitory immune checkpoint that is increased after ipilimumab therapy in patients with prostate cancer. *Nat Med*. 2017;23:551–555.
77. Schaafsma E, Croteau W, ElTanbouly M, et al. VISTA targeting of T-cell quiescence and myeloid suppression overcomes adaptive resistance. *Cancer Immunol Res*. 2023;11:38–55.